Drought and Persistent Wet Events Projected in the CMIP5 Experiments

Lindsey N. Long[1,2], Kingtse C. Mo[1] and Jae-Kyung E. Schemm[1]
[1]Climate Prediction Center, NCEP/NWS/NOAA
[2]Wyle Laboratories

Submitted to J. Climate

Special issue on CMIP5 experiments

Corresponding author: Lindsey Long, Climate Prediction Center, NCEP/NWS/NOAA, 5200 Auth Rd, Camp Springs, MD: Email: Lindsey.Long@noaa.gov

Abstract

CMIP5 historical experiments are examined to assess the ability of models to simulate drought and persistent wet events over the United States. A total of 14 models are selected for this study. They are CanESM2, BCC-CSM1.1, CCSM4/RSMAS, CNRM-CM5, CSIRO-Mk3.6.0, GISS-E2-H, GFDL-ESM2G, HadGEM2-ES, IPSL-CM5A-LR, MIROC4h, MIROC-ESM, MPI-ESM-LR, MRI-CGCM3, and NorESM1-M. The models have different skill in simulating the frequency of occurrence (FOC) of persistent precipitation and soil moisture anomalies. Extreme events should be more (less) persistent over the western (eastern) United States. Only the CCSM4 model is able to fully capture the east-west contrast of the hydroclimate regimes. Most models either have too few persistent extreme events or they misplace the maxima over the southern Plains. The models which are able to capture the rough locations of maxima also have a realistic climatology for precipitation and are able to capture the influence of ENSO on precipitation over the United States.

The response by extreme events to an increase in CO_2 using the RCP 4.5 and RCP 8.5 projection experiments is also analyzed. The differences in FOC between the projection and historical experiments are small when each experiment's own climatology is used; however, the differences are large when the climatology of the historical experiment is used for both experiments. Most models show some decrease (increase) in wet (dry) events in Mexico and the Southwest and an increase (decrease) in wet (dry) events in the northeastern and eastern United States. Results are also similar to the previous assessment of the CMIP 3 experiments.

1. Introduction

Climate change projections from coupled atmosphere-ocean-land models show significant decadal variability. For North America, one of the major conclusions from the Intergovernmental Panel on Climate Assessment Report Four (IPCC AR4) is that drought will occur more often over the Southwest, northeastern Mexico, the Caribbean and the adjacent land areas while persistent wet events will occur over the Northeast (Seager et. al 2007, Seager and Vecchi 2010). The drying in the Southwest is attributed mainly to the poleward expansion of the dry zone in the subtropics, while the wetness over the Northeast is due to the northward movement of the storm tracks. These changes are results of differences in the climatology.

The change in drought occurrence can also be influenced by changes in the oceanic variability and the atmospheric responses to these changes. For example, the World Climate Research Programme (WCRP) Coupled Model Intercomparison Project 3 (CMIP3) 21st Century Special Report for Emission Scenario (SRES) A1B experiments show that there is a change in the sea surface temperature (SST) variability in the Tropical Pacific. The SRES A1B experiments simulated climate change with CO_2 concentration of about 700 ppm by 2100 (Meehl et al. 2009). Yeh et al. (2009) reported that a change in the mean thermocline depth leads to a change in ENSO characteristics in the SRES A1B experiments. Therefore, there will be more frequent occurrences of the central Pacific ENSO, with the center of warm SST anomalies (SSTAs) located in the central Pacific, and less occurrences of the traditional ENSO, with the warmest SSTAs located in the eastern Pacific. Their ENSO events were defined according to the Nino 3 and Nino 4 SST indices during winter in the 20th century historical simulations and in the SERS A1B projections. Precipitation over the United States will respond differently to these two

types of ENSO (Mo 2010). Therefore, the changes in the variability of SSTAs can also impact extreme events.

There are two very different hydroclimate regimes over the United States; drought and persistent wet events are more likely to occur over the western interior states and less likely to occur over the east. Mo et al. (2012) examined the ability of the CMIP3 models in the 20th century historical simulations for the IPCC AR4 and the National Centers for Environmental Prediction (NCEP) Climate Forecast System (CFS) models to simulate drought occurrence. They found that only the higher resolution CFS models are able to capture the east-west contrast of the hydroclimate over the United States. These models also have a realistic seasonal cycle and are able to capture the P responses to ENSO. Overall, most CMIP3 models are not able to capture this east-west contrast. If most models cannot simulate realistic drought over the United States historically, will their projections be reasonable?

To address the scientific questions that arose from the IPCC AR4 and to have a better understanding of the decadal variability, the WCRP's working group on coupled modeling designed the CMIP Phase 5 (CMIP5) experiments (Meehl et. al. 2009, Taylor at el. 2012). One of the objectives of the CMIP5 experiments is to evaluate how realistic the simulations are and provide guidance on future projections of climate change. There is a comprehensive and coherent effort to diagnose and evaluate the CMIP5 historical experiments over the United States (Sheffield et al. 2012a, Sheffield et al. 2012b) and assess the 21st century projections over North America (Maloney et al. 2012) organized by the NOAA Modeling, Analysis, Predictions, and Projections (MAPP) Program CMIP5 Task Force.

In this paper, we will focus on persistent drought and wet events over the United States. One advantage of the CMIP5 experiments is that the models have a higher resolution than the

93 CMIP3 experiments (Taylor et al. 2012). The higher resolution should improve the ability of
94 models to simulate a realistic hydrologic cycle and the occurrence of these extreme events.
95 Therefore, our objectives are (1) to document the ability of the CMIP5 models to capture the
96 frequency of occurrence of persistent extreme events in the historical experiments, (2) to
97 investigate the projections by looking at the mechanisms behind the changes in the FOC of
98 extreme events with increases in CO_2 and (3) to recommend whether the projected changes are
99 realistic.

100 **1. Data and Procedures**

101 **a) Observations**

102 The observational data sets used for this study are the same as those used in Mo et al.
103 (2012) for P and soil moisture, but updated to 2010. We review them briefly here for
104 completeness. Two observed P datasets are used: monthly P from the University of Washington
105 (UW) for the period from 1915 to 2010 and the monthly mean Climate Prediction Center (CPC)
106 unified P data (Xie et al. 2010) which covers the period from 1950 to 2010. The horizontal
107 resolution for both datasets is 0.5 degrees. Each dataset is treated as one member of the P
108 ensemble.

109 Soil moisture (SM) data are taken from the North American Land Data Assimilation
110 Systems (NLDAS) from the UW (Wang et al. 2009) because no long term observed data set is
111 available. The SM ensemble members are outputs from three land surface modals (LSMs):
112 Variable Infiltration Capacity model (VIC) (Liang et al. 1994, 1996), Noah (Koren et al. 1999,
113 Ek et al. 2003), and Sacramento (SAC) (Burnash 1973). The dataset covers the period from 1916
114 to 2006. The SM time series from each NLDAS model simulation is considered one member of
115 the SM ensemble.

116 **b) CMIP5 Model Simulations**

117 For this study, fourteen models are examined from the CMIP5 submissions. They are the
118 CanESM2 (CAN), CCSM4/RSMAS (CCSM4), CSIRO-Mk3.6.0 (CSIRO), IPSL-CM5A-LR
119 (IPSL), MPI-ESM-LR (MPI), BCC-CSM1.1 (BCC), CNRM-CM5 (CNRM), GFDL-ESM2G
120 (GFDL), HadGEM2-ES (HadGEM2), MRI-CGCM3 (MRI), NorESM1-M (NCC), MIROC-
121 ESM, MIROC4h, and GISS-E2-H (GISS). The model output is available from the Program for
122 Climate Model Diagnosis and Intercomparison (PCMDI) at their web site
123 http://www.pcmdi3.llnl.gov/esgcet/home.htm.

124 Three experiments are utilized in this study at a monthly temporal resolution. The
125 historical experiment covers the period from 1850 to 2005, and the Representative Concentration
126 Pathway (RCP) 8.5 and RCP 4.5 projection experiments cover the period from 2006 to 2100.
127 The historical experiment is used as a control run for the 20th century to define the current
128 climatologies of the model. The two projection simulations are used to show a "high emissions
129 scenario" with the RCP 8.5 projection and a "midrange mitigation emissions scenario" with the
130 RCP 4.5 projection (Taylor et al. 2012). For the RCP 8.5 experiment, modelers were asked to
131 slowly increase the amount of CO_2 in the atmosphere during the 94-year period until the CO_2
132 level reached four times current levels in 2100. The RCP 4.5 experiment, which calls for a
133 doubling of CO_2 instead of a quadrupling similar to the CMIP3 SRES A1B experiment, is also
134 used here as a comparison to the RCP 8.5 experiment. Additional information on the
135 experiments can be found in the CMIP5 Experiment Design report (http://cmip-
136 pcmdi.llnl.gov/cmip5/) and in Taylor et al. (2012).

137 Each model submission varies in resolution and number of ensemble members. This
138 information and each model's institution are presented in Table 1. Resolutions between models

range from 3.75 x 1.89 degrees to 0.56 degrees. Two models, MIROC4h and GISS-E2-H, do not have RCP 8.5 experiment submissions that coincide with the historical experiment physics and are therefore omitted from the portion of this paper dealing with projections. Also, many of the models only have one RCP 8.5 submission. Because multiple ensemble members are ideal for this analysis, the first five models listed in Table 1, CanESM2, CCSM4, CSIRO-Mk3.6.0, IPSL-CM5A-LR and MPI-ESM-LR, which have three or more members for each experiment, are the focus of the later portion of this paper.

c) Drought Classification

In this paper, we will analyze both meteorological drought, measured by P deficit, and agricultural drought, measured by SM deficit (Keyantash and Dracup 2002). The drought index used to classify meteorological drought is the 6-month Standardized Precipitation Index (SPI6) while soil moisture percentiles are used to classify agricultural drought (Mo 2008).

The procedures used to calculate drought indices are described in Mo et al. (2012). Therefore, the description here will be brief. For observations, the SPI6 is computed from the two P data sets, and SM anomaly percentiles are computed for each member of the SM NLDAS outputs. The same drought indices are computed for each member of the CMIP5 experiments using P and SM.

For a given experiment, we append the time series of SPI6 (or SM percentiles) from each member together to form one long time series. N_{total} is the total months of runs from a given experiment or the length of an observed data set. At each grid point, an extreme negative (positive) event is selected when the SPI6 index or the SM percentile is below (above) a certain threshold. The threshold for SPI6 is -0.8 (0.8) for a dry (wet) event (Svoboda et al. 2002). The threshold for the SM percentile is 20% (80%). At each grid, the number of months (N) that

extreme events occur is 20% of the record length. (N/N_{total} = 20%). Because an extreme drought (persistent wet) event means persistent dryness (wetness), a drought (wet) episode is selected when the index is below (above) this threshold for 3 consecutive seasons (9 months) or longer. The number of months that an extreme event persists for more than 9 months is labeled as N_p. The frequency of occurrence of drought or persistent wet spells (FOC) is defined as the ratio between the number of persistent extreme events and the total number of extreme events:

$$FOC = N_p/N. \quad \text{Eq. (1)}$$

d) ENSO composites

ENSO composites are calculated using El Nino (warm) and La Nina (cold) seasons. These seasons are selected using the Nino 3.4 Index, which is defined as the SSTAs averaged over 5^oS-5^oN and 170^o-120^oW, normalized by the monthly mean standard deviation, and averaged over a 3-month period. A season (JFM, AMJ, JAS, and OND) is defined as an El Nino (La Nina) season if the value is above (below) a 1.0^oC threshold. Normally a threshold of $0.5\ ^oC$ would be used; however, the ENSO signal in the models appears to be very strong. Therefore a more stringent criterion is used to select seasons with the strongest ENSO signal. Once a season is defined, all El Nino (La Nina) years for each season are averaged together for a given variable (SSTA or SPI6) to form the seasonal composites. The composite for each season can then be averaged together to create an annual ENSO composite for both warm and cold events. Therefore, the same events are used for both the SSTA and SPI6 composites.

For observations, a season is defined as El Nino or La Nina using the CPC historical Oceanic Nino Index (ONI) - http://www.cpc.ncep.noaa.gov/products/analysis_monitoring/ensostuff/ensoyears.shtml

These values are based on SST anomalies in the Nino 3.4 region using a 0.5 ^{o}C threshold. The SST data used to calculate the composites are from the Climate Data Assimilation System (CDAS) which is part of the NCEP/NCAR Reanalysis Project (Kalnay et al, 1996). Monthly data is used from 1950 to 2011.

2. Simulation of historical experiments

a) Frequency of occurrence

Over the United States, there are two hydroclimate regimes. As seen in Fig. 1f, the western interior regime west of 95^{o}W is relatively dry. In this area, the vegetation is sparse and the water holding capacity is large. Both P and SM anomalies are more likely to persist (Mo and Schemm 2008). In the eastern United States, it rains often with an annual rainfall of more than 4 mm day^{-1}. Therefore, dryness in one season is likely to be relieved in the next season, and anomalies are less likely to persist. Most models do fairly well in capturing the maxima in P in the Southeast and Pacific Northwest regions, although exact locations vary (Fig. 1). The models show more variability when looking at the dryness in the interior. They all tend to show less P in the region, but most models are still too wet. Only the CAN, CSIRO, IPSL, MPI, and HadGEM2 models show P values dropping to below 1.5 mm day^{-1} in the western interior. These two regimes of wetness in the east and dryness in the west create the east-west contrast that is the signature of the FOC of persistent wet and dry events for both meteorological drought classified by SPI6 (Fig. 2f) and agricultural drought classified by SM percentiles (Fig. 3f).

The observed FOC of extreme events based on SPI6 (Fig. 2f) shows a band of maxima over the western interior states. It also shows another band of maxima extending from Nevada and Utah to the Southwest and Texas. Persistent events are also found over the Great Plains

with a weaker maximum located in Kansas. In Fig. 2, both the CCSM4 and CAN models capture the east-west contrast, although magnitudes of the FOC are too weak for the CAN. The MPI also captures the signal with one maximum located at Utah and another one over the Great Plains, but the second maximum over the Great Plains is too strong in comparison with observations. This is an improvement in comparison to the MPI CMIP3 simulation (Mo et al. 2012). For the CMIP3 model, the MPI only shows one maximum located over the Southern Plains. The MRI shows weak maxima centered over Nevada and the Four Corners, but the pattern is less organized. The NCC and MIROC_ESM show a band of maxima over the Southwest, but the FOC north of 40^{o}N is too weak. The MIROC4h is a high resolution model with 0.56^{o} resolution but P is very noisy. It does not capture the east-west contrast, but it does show large values over the western interior regime. The extreme events simulated by the MIROC4h tend to persist for only 4-6 months instead of 9 months. The remaining models fail to capture any hint of the east-west contrast. The IPSL, CNRM, and GISS have maxima located over the Gulf region, while the CSIRO, BCC, and GFDL models mostly have a maximum over the Southern Plains. The GFDL model also has an additional maximum over the upper Missouri river basin in Montana, and the FOC is very similar to the CMIP3 historical experiment results. The worst model is the HadGEM2 which has anomalies that are too weak. This is because the anomalies do not persist long enough to be counted as persistent events.

It is interesting to note that although a model can capture the FOC for the meteorological drought, it may not simulate the agricultural drought classified by SM (Fig. 3). For SM, the FOC from the NLDAS shows that persistent anomalies are located over the region west of 90^{o}W (Fig. 3f). The SM FOC in the CAN model, which also did well in simulating FOC for the meteorological drought, shifts the maximum to the central United States (Fig. 3a). This is also

true for the HadGEM2, MRI, NCC and GISS models. Some models that failed to capture the east-west contrast in the meteorological drought do better with the agricultural drought, such as CSIRO, CNRM, MIROC-ESM, and MIROC4h. IPSL and BCC do not have enough persistent extreme events, while GFDL has too many over the entire United States. The best performing model in simulating the FOC for agricultural drought is the MPI model. It captures the east-west contrast and also has realistic magnitudes. The CCSM4 model, which performs best for meteorological drought, has some indications of the east-west contrast, but there are too many events along the Gulf Coast and the North-Central United States.

b. **Diagnostics**

In this section, we will examine the ability for models to capture a realistic climatology and the response to ENSO. Mo et al. (2012) demonstrate that models that capture the east-west contrast of FOC are also models that have realistic P climatology and are able to capture the influence of ENSO over P in the United States.

One reason that extreme events over the western interior region persist is that the region is very dry with an annual mean P of less than 1-1.5 mm day^{-1} (Fig. 1f). Also the region has a very weak seasonal cycle (Fig. 4f). It does not rain often, and once drought occurs, it tends to persist. This is in stark contrast to the East. As discussed early in Fig. 1, many models tend to be too wet in the western interior. The CAN and CCSM4 models which have more realistic SPI6 FOC also have a realistic P climatology. Fig. 4 shows the magnitude of the P seasonal cycle estimated by the difference between P maximum and P minimum divided by 2. Both the interior western region and eastern United States have very weak seasonal cycles, with stronger signals over the central United States and Pacific coast. Most models do very poorly in simulating the seasonal cycle. They tend to do well over the Pacific coast, but the maxima over the central

253 United States is usually too far west and is too strong in the Southeast; however, there does seem
254 to be an improvement over the CMIP3 models (Mo et al. 2012).

255 ENSO is the major forcing that regulates the precipitation over the United States. Mo
256 (2011) studied the relationships between drought and ENSO and found that drought over the
257 southern Plains, Mississippi River Basin and the Gulf States is most likely to occur during cold
258 ENSO events. Here, composites are used to examine the ability of models to simulate ENSO and
259 the SPI6 responses.

260 Fig. 5 shows the composite difference of surface temperature anomalies between cold
261 and warm ENSO events in the historical experiments. The observations show negative
262 anomalies extend from the eastern Pacific to the dateline in the central Pacific (Fig. 5f). Almost
263 all models have an ENSO signal except for the MIROC-ESM which shows very weak composite
264 differences. One of the common errors found in the CMIP3 models is that the simulated SSTAs
265 associated with ENSO extend to the western Pacific and the maritime continent (Joseph and
266 Nigam 2006). This extension will influence the responses to ENSO downstream. Most CMIP5
267 models still show this same problem with SSTAs extending too far west. Only five models, the
268 BCC, CNRM, HadGEM2, MRI, and NCC, have anomalies extending only to the dateline. The
269 HadGEM2 also seems to have a cold pool in the Northern mid-latitudes which is not seen in
270 observations or any of the other models.

271 The errors in SSTAs associated with ENSO should impact the P and SPI6 responses. The
272 SPI6 composites between cold and warm events are given in Fig. 6. The ENSO composite for
273 observations (Fig. 6f) shows dryness over the southern United States with a band of maxima
274 extending from Utah and Colorado to New Mexico and Texas. There is also wetness in the
275 Northwest and over the Ohio River Valley. Note that because the signal is somewhat weak in

276 the models, we chose not to mask out values with significant levels below 5% significance.
277 Most models show dryness over the southern United States and a little over half show wetness in
278 the Northwest; however, the magnitudes of the composite are too weak. Only the NCC shows
279 any wetness near the Ohio River Valley. Both the CAN and CCSM4 models capture the
280 responses to ENSO well, and these two models also have realistic FOCs (Fig. 2). In addition to
281 these two models, the CSIRO, MRI, and NCC also show dryness over the western states with
282 weaker magnitudes. They also show a hint of correspondence between the SPI6 ENSO
283 composites and the SPI6 FOCs. Although the HadGEM2 model has an ENSO signal in the
284 Tropics, it does not capture the response in SPI6. This is consistent with its inability to capture
285 the SPI6 FOC. For a model to capture the FOC of extreme events for meteorological drought it
286 not only has to have a realistic ENSO signal in SSTAs in the tropical Pacific, it also needs to
287 capture the P responses to ENSO.

288 It is interesting that the model that best captures the FOC of the extreme events for
289 meteorological drought is not necessary the best model that captures the FOC for agricultural
290 drought. To capture the FOC for agricultural drought, which is based on the soil moisture
291 percentiles, the model needs to capture the persistence of SM. Fig. 7 shows the characteristic
292 time, T_o, computed based on the SM anomalies in months (Trenberth 1984). The T_o value
293 represents persistence of SM. It estimates the time it takes for SM to overcome the impact of the
294 initial conditions. For the NLDAS, T_o shows the east-west contrast over the United States. Over
295 the western region, T_o is longer than 2 years. Over the eastern United States, T_o is less than 6
296 months; however, this is still longer than the persistence of P. The persistent nature of SM is the
297 reason that once a region is under agricultural drought, it takes the SM in the region a long time
298 to recover. There is a good correspondence between T_o (Fig. 7) and FOC for the agricultural

299 drought (Fig. 3). The best simulations are from the CAN, CSIRO, MPI and GISS; they capture
300 the pattern and magnitudes well. For many models, the maxima shift too far east. The IPSL and
301 BCC models have weak, unrealistic simulations for the persistence of SM and they do not
302 capture the FOCs for the extreme events.

303 Overall, most models are not able to capture the FOC of extreme events for either
304 meteorological or agricultural drought. The question is whether the poor performance of the
305 model will influence its ability to predict the influence of rising CO_2 in the projections? The
306 answer to this question depends on the mechanisms responsible for changes in the projections.

307 **3. The 21th Century Projection Experiments**

308 **a) Changes in FOC**

309 In this section, we will examine the changes of FOC for meteorological and agricultural
310 droughts due to the increase of CO_2 projected by both the RCP 4.5 and RCP 8.5 experiments.
311 There are two possibilities as to why the FOCs change between the RCP and historical
312 experiments: 1) there is a change in climatology or 2) there are changes in oceanic and
313 atmospheric circulations which in turn influence the occurrence of drought. If the climatology is
314 the cause, the model only has to simulate the climatological differences between the two
315 experiments to have realistic projections of the FOC for extreme events. As found in the SRES
316 A1B experiments, the SSTA and atmospheric variability may also change due to the increase of
317 CO_2 (Yeh et al. 2009). This will then change the behavior of the extreme events over the United
318 States. In this case, the model will be required to capture the different responses to these
319 changing ENSO events in order to have a realistic projection.

320 Both changes in climatology and changes in variability can impact the FOC over the United
321 States, and they can occur simultaneously. To examine these two causes, we compute SPI6 from

322 P for the RCP 4.5 and RCP 8.5 experiments using their own projected monthly mean P
323 climatology. The differences between the FOC for the historical experiments and the projection
324 experiments represent changes due to SSTA variability including the changes in the ENSO
325 modes. As discussed in Section 2, only five models are used to investigate the projections. The
326 other models either did not have projection submissions or did not have enough members to
327 create a long enough time series. Short time series do not have enough extreme events for
328 significant results. Fig. 8 shows the SPI6 FOC differences between the RCP 8.5 experiments and
329 the historical experiments where the P anomalies are based on each experiment's own
330 climatology for positive (wet, left panel) and negative (dry, right panel) events. There are very
331 few differences over the United States. None of the difference maps can pass the field
332 significance test. The differences using the RCP 4.5 experiments show similar results (not
333 shown). This implies that once the model reaches equilibrium, the responses to the changes in
334 SSTA variability in the new climate are small. Of course, there is also a possibility that the
335 models do not capture the changes in SSTA modes or the responses to them.

336 The differences in SPI6 FOC between the RCP 8.5 or RCP 4.5 experiments and the historical
337 experiments are again shown in Fig. 9 for positive extreme events and Fig. 10 for negative
338 extreme events. With these plots, anomalies are computed according to the climatology of the
339 historical experiments for all three experiments. Therefore, the changes of FOCs are due to the
340 difference in climatology between the historical and projection experiments. There is symmetry
341 between the changes in FOCs for the positive and negative events. With the increase of CO_2,
342 most of the models show an increase (decrease) in the occurrence of drought (persistent wet
343 events) over the Southwest and Northern Mexico and a decrease (increase) in the occurrence of
344 drought (persistent wet events) over the Northeast and the northern United States. As discussed

345 in the introduction, this dryness in the southwest and wetness over the Northeast are consistent
346 with results reported in the WCRP AR4 (Seager et al. 2007). The general picture is similar for
347 the five models, but the details differ. For example, the CAN and IPSL models show an increase
348 of wet events over the Pacific Northwest (Fig. 9), but the CSIRO and MPI models show little to
349 no increase. Overall, the differences between RCP 4.5 and RCP 8.5 are very similar with RCP
350 8.5 differences being only slightly stronger. This implies that after the CO_2 amounts reach a
351 certain threshold, additional CO_2 will have little effect on the persistent behavior of the extreme
352 events.

353 Fig. 11 shows the differences in SM FOC between the RCP 8.5 and historical
354 experiments with positive events on the left and negative events on the right. Again, only the
355 historical climatology is used to calculate anomalies. The CCSM4 model has been removed
356 from this plot because the CO_2 increase is not included in the SM projection. Therefore, the
357 historical and projection climatologies are the same for the CCSM4 model. There are some
358 similarities between the SPI6 and SM FOCs but also many differences. All models show some
359 decrease in the occurrence of positive events in the Southwest and northern Mexico which is
360 consistent with the SPI6 FOC plots. However, the models show these decreases extending up
361 through the northwestern interior into Canada. In addition, all models show little to no change in
362 the eastern or northeastern United States whereas the SPI6 FOC plots show significant increases
363 in wet events. The SM FOC for negative events also shows a similar picture in the southwest
364 with negative events increasing in frequency in most models; however these increases stretch
365 into the central United States and farther east in all models but the CAN which shows a decrease
366 in extreme drought events for most of the United States.

Overall, the conclusion from the CMIP3 experiments pertaining to increased drought in the southwest and wet events in the Northeast still holds for the CMIP5 experiments. However, unlike in the CMIP3 projections, the differences in the SPI6 and SM patterns are due to changes in climatology and not a result of changes to the ENSO pattern caused by SSTA variability.

b) **Changes in P and Atmospheric Circulation**

Since the climatology plays an important role in determining the changes in FOC, we will examine whether the P climatology difference between the historical and projected experiments has the same signature for the other models which did not have long enough records or enough ensemble members to compute the FOC. Figure 12 shows the annual P mean difference. There are differences from one model to another, but all of them show that RCP 8.5 experiments overall are drier over the Southwest and Northern Mexico and wetter over the Northeast and the Northern Unites States. The one exception is the CAN model which shows only weak dryness in Eastern Mexico and Texas and wetness along the Pacific coast. This is also evident in the FOC plots in Figs. 9 and 10. This is further evidence that models need to get the change in climatology correct to simulate the change in FOC. Similar differences are also observed in the RCP 4.5 experiments (not shown). These results are consistent with Fig. 1 in Maloney et al. (2012) which shows that in the CMIP5 13-model ensemble the dryness in the southwest and the wetness in the northeast are mostly winter features, although dryness is also evident in the summer farther south in Central America. The models also show significant agreement in these areas during both seasons (Fig. 2, Maloney et al. 2012).

We have shown that the changes in FOCs between the RCP 8.5 or RCP 4.5 experiments and historical experiments are due to the changes in climatology between the historical experiment and the projections. All models show a similar pattern in P climatological differences. Therefore,

390 even though models are not able to capture the FOC of extreme events, the projections can still
391 be trusted.

392 The changes in P climatology can be linked to warming in the tropical oceans. Fig. 13
393 displays the differences in the mean P climatology (left) and SSTA climatology (right) between
394 the RCP 8.5 and historical experiments during the winter months of January to March (JFM) as
395 an example. All five models show warming in the global ocean. In the Tropics, the differences
396 can be 1-3 ^{o}C which are as large as the warming during a typical warm ENSO event. With
397 warming in the Tropics, there is increased convection and more positive P differences between
398 the RCP 8.5 and historical experiments. The largest positive P differences are in the tropical
399 Pacific along the equator and are mostly co-located with the largest temperature increases. In
400 addition, all models show dryness over Central America and just north of the increased P near
401 the equator. With rising motion from the enhanced convection in the tropical Pacific, the
402 downward branch of the Walker circulation is located over Central America. And with strong
403 precipitation anomalies in the Tropics, the enhancement of the Hadley circulation may cause the
404 expansion of the subtropical dry zone, which includes the southwest United States, in response to
405 increases in SSTAs. All models show this expansion of the dry zone which is similar to results
406 seen in the CMIP3 experiments (Seager et al. 2007). The increased wetness in the Northeast is
407 also seen in the CMIP3 results (Seager and Vecchi 2010). Fig. 13 in Maloney et al. (2012)
408 shows that this may be caused by a shift in the storm tracks northward in the RCP 8.5
409 projections. Their Fig. 13 uses a 16-member ensemble of CMIP5 models to show the winter
410 storm track activity increasing over most of North America at the 250 hPa level. The increase in
411 storm track activity is pushed farther north into Canada during the summer months, and there is a
412 decrease in activity over the United States. This is consistent with our analysis which found that

413 the increased wetness in the Northeast is dominated by the winter months and not nearly as
414 substantial during the summer (not shown).

415 **4. Conclusions**

416 In this paper, we have examined the ability of the CMIP5 models to capture the FOC of
417 extreme events. To do this, 14 models were chosen from the CMIP5 submissions. Only the
418 CCSM4 model fully captures the observed SPI6 FOC with a band of maxima extending from
419 Nevada to western Texas. The CAN and MRI models have maxima over the western region, but
420 the magnitudes are too weak. The MPI model captures the maximum over the western region,
421 but the second maximum located over the Southern Plains is too strong. The CCSM4 model also
422 has realistic P climatology and is able to capture the responses to ENSO. All models except the
423 MIROC-ESM have a realistic ENSO signature, but not all models are able to capture the P
424 responses to ENSO events.

425 The changes between the RCP and historical experiments were analyzed, and it was
426 found that there is little change in FOC when the RCP climatology is used for the RCP
427 experiments, but that large changes occur when the historical climatology is used to calculate
428 anomalies for FOC. Therefore, the differences in FOC are mainly due to changes in climatology.
429 The changes in the SSTA variability do not seem to play an important role. Therefore, the model
430 projections can be trusted. The biggest changes in climate from the historical to the projection
431 experiments are the increased dryness and occurrence of drought in the southwest United States
432 and wetness over the Northeast. This is consistent with results from the CMIP3 experiments.

433 The differences between the RCP 4.5 and RCP 8.5 experiments were also analyzed. The
434 differences in FOCs when comparing the RCP 4.5 and RCP 8.5 experiments are small. This

implies that once the CO_2 reaches a certain threshold, there is little change in the occurrence of extreme events.

Finally, increases in CO_2 cause the SSTs in the tropical oceans to increase between 1-3 ^{o}C which then causes precipitation and convection to increase in the tropical Pacific. The strengthening of the Hadley circulation expands the dryness in the subtropics. This then causes dryness over the Caribbean, Central America, and the Southwest. The northward shift in the storm tracks also may increase the wetness over the Northeast.

Acknowledgements

The authors would like to acknowledge the modelers who participated in the CMIP5 experiments and those who maintained the data portal for all their time and effort. This work was supported by the NOAA Climate Program Office Modeling, Analysis, Predictions and Projections (MAPP) Program as part of the CMIP5 Task Force under grant #K8R1RP3.

References

Burnash, R. J., R. J. Ferral, and R. A. McGuire, 1973: A generalized streamflow simulation system. Conceptual modeling for digital computers. Technical report, 204pp. Joint Fed. And State River Forecast Center, Sacramento, CA.

Ek, M. B., K. E. Mitchell, Y. Lin, E. Rogers, P. Grunmann, V. Koren, G. Gayno, and J. D. Tarpley, 2003: Implementation of Noah land surface model advances in the National Centers for Environmental Prediction operational mesoscale Eta model. *J. Geophys. Res*., **108 (D22**), 8851. DOI:10.1029/2002JD003296.

Joseph, R. and S. Nigam, 2006: ENSO evolution and teleconnections in IPCC Twentieth Century climate simulations: Realistic representation? *J. Climate*, **19**, 4360-4377.

Kalnay, E. and Coauthors, 1996: The NCEP/NCAR 40-year reanalysis project. *Bull. Amer. Meteor. Soc.*, **77**, 437–471.

Keyantash, J. and J. A. Dracup, 2002: The quantification of drought: An evaluation of drought indices. *Bull. Amer. Meteor. Soc.*, **83**, 1167-1180.

Koren, V., J. Schaake, K. Mitchell, Q. Duan, F. Chen, and J. Baker, 1999: A parameterization of snowpack and frozen ground intended for NCEP weather and climate models. *J. Geophys. Res.*, **104**, 19569-19585.

Liang, X., D. P. Lettenmaier, E. F. Wood, and S. J. Burges, 1994: A simple hydrologically based model of land surface water and energy fluxes for GCMs. *J. Geophys. Res.*, **99**, 14415-14428.

Liang, X., D. P. Lettenmaier, and E. F. Wood, 1996: One-dimensional statistical dynamic representation of subgrid spatial variability of precipitation in the two-layer variable infiltration capacity model. *J. Geophys. Res.*, **101**, 21403-21422.

Maloney, E. D. and Coauthors, 2012: North American climate in CMIP5 experiments: Part III: Assessment of 21st Century projections. *J. Climate*, Submitted July 2012.

Meehl, G. A. and Coauthors, 2007: The WCRP CMIP3 multimodel dataset: A new era climate change research. *Bull. Amer. Meteor. Soc.*, **88**, 1383-1394.

Meehl, G. A. and Coauthors, 2009: Decadal prediction. Can it be skillful? *Bull. Amer. Meteor. Soc.*, **90**, 1467-1485. DOI:10.1175/2009BAMS2778.1.

Mo, K. C., 2008: Model based drought indices over the United States. *J. Hydrometeor*., **9**, 1212-1230.

Mo, K. C. and J. E. Schemm, 2008: Drought and persistent wet spells over the United States and Mexico. *J. Climate*, **21**, 980-994.

Mo, K. C., 2010: Interdecadal modulation of the impact of ENSO on precipitation and temperature over the United States. *J. Climate*, **23**, 3639-3656.

Mo, K. C., 2011: Drought onset and recovery over the United States. *J. Geophys. Res.*, **116**, D20106, DOI:10.1029:/2011JD016168.

Mo, K. C., L. N. Long, and J. E. Schemm, 2012: Characteristics of drought and persistent wet spells over the United States in the atmosphere-land-ocean coupled model experiments. *Earth Interact*., In press.

Seager, R. and Coauthors, 2007: Model projections of an imminent transition to a more arid climate in Southwestern North America. *Science,* **316**, 1181-1184.

Seager, R. and G. A. Vecchi, 2010: Greenhouse warming and the 21th central hydroclimate of southwestern North America. *Proc. Nat. Acad. Sciences*, **107**, 21277-21282.

Sheffield, J. and Coauthors, 2012a: North American climate in CMIP5 experiments: Part I: Evaluation of 20th Century Continental and Regional Climatology. *J. Climate*, Submitted July 2012.

Sheffield, J. and Coauthors, 2012b: North American climate in CMIP5 experiments: Part II: Evaluation of 20th Century Intra-Seasonal to Decadal Variability. *J. Climate*, Submitted July 2012.

Svoboda, M. D. and Coauthors, 2002: The drought monitor. *Bull. Amer. Meteor. Soc.*, **83**, 1181-1190.

Taylor, K. E., R. J. Stouffer and G. A. Meehl, 2012: An overview of CMIP5 and the Experimental design. *Bull. Amer. Meteor. Soc.*, **93**, 485-498.

Trenberth, K. E., 1984: Some effects of finite sample size and persistence on Meteorological statistics. Part II: potential predictability. *Mon. Wea. Rev.*, **112**, 2369-2379.

Wang, A., T. J. Bohn, S. P. Mahanama, R. D. Koster, and D. P. Lettenmainer, 2009: Multi model reconstruction of drought over the continental United States. *J. Climate*, **22**, 2684-2712.

Xie, P. P., M. Chen, and W. Shi, 2010: CPC unified gauge based analysis of global daily precipitation. *24th Conf. on Hydrology*, Atlanta, GA, Amer. Meteor. Soc., Jan 18-21, 2010.

511 Yeh, S. W., J. S. Kug, B. Dewitte, M. H. Kwon, B. P. Kirkman and F. F. Jin 2009: El Nino in a
512 changing climate, *Nature*, **461**, 511-514. DOI:10.1038/nature08316.

513

Model	Organization	Resolution (degrees)	Historical Period	Historical Members	RCP 8.5/4.5 Members
CanESM2 (CAN)	Canadian Centre for Climate Modelling and Analysis	2.8		5	5 / 5
CCSM4/ RSMAS (CCSM4)	NCAR, University of Miami	1.25 x 0.94		6	5 / 5
CSIRO-Mk3.6.0 (CSIRO)	Commonwealth Scientific and Industrial Research Organization/ Queensland Climate Change Centre of Excellence	1.875		10	10 / 10
IPSL-CM5A-LR (IPSL)	Institut Pierre-Simon Laplace	3.75 x 1.89		4	4 / 4
MPI-ESM-LR (MPI)	Max Planck Institute for Meteorology	1.875		3	3 / 3
BCC-CSM1-1 (BCC)	Beijing Climate Center, China Meteorological Administration	2.8		3	1 / 1
CNRM-CM5 (CNRM)	Centre National de Recherches Meteorologiques / Centre Europeen de Recherche et Formation Avancess en Calcul Scientifique	1.4		9	5 / 1 (0)
GFDL-ESM2G (GFDL)	NOAA Geophysical Fluid Dynamics Laboratory	2.5 x 2	1861-2005	3 (1)	1 / 1
HadGEM2-ES (HadGEM2)	Met Office Hadley Centre	1.875 x 1.25	1860-2005	4	4 / 4
MRI-CGCM3 (MRI)	Meteorological Research Institute	1.125		3	1 / 1
NorESM1-M (NCC)	Norwegian Climate Centre	2.5 x 1.89		3	1 / 1
MIROC-ESM	Atmosphere and Ocean Research Institute (University of Tokyo), National Institute for Environmental Studies, & Japan Agency for Marine-Earth Science and Technology	2.8		3	1 / 1
MIROC4h		0.56	1950-2005	3	0 / 3
GISS-E2-H, p2 (GISS)	NASA Goddard Institute for Space Studies	2.5 x 2		5	0 / 0

Table 1: CMIP5 Experiment Information. Historical period given if it differs from the 1850-2005 period. If the number of soil moisture members differs from the other variables, it is included in parenthesis.

Figure Captions

Fig. 1: Annual mean P for a) CanESM2, b) CCSM4, c) CSIRO-Mk3.6.0, d) IPSL-CM5A-LR, e) MPI-ESM-LR, f) Observations, g) BCC-CSM1.1, h) CNRM-CM5, i) GFDL-ESM2G, j) HadGEM2-ES, k) MRI-CGCM3, l) NorESM1-M, m) MIROC-ESM, n) MIROC4h, and o) GISS-E2-H climatology for the historical experiments. Contour interval is given by the color bar.

Fig. 2: Frequency of occurrence (FOC) of extreme events that persist more than 9 months based on SPI6 index averaged over positive and negative events for a) CanESM2, b) CCSM4, c) CSIRO-Mk3.6.0, d) IPSL-CM5A-LR, e) MPI-ESM-LR, f) Observations, g) BCC-CSM1.1, h) CNRM-CM5, i) GFDL-ESM2G, j) HadGEM2-ES, k) MRI-CGCM3, l) NorESM1-M, m) MIROC-ESM, n) MIROC4h, and o) GISS-E2-H for the historical experiments. Contour interval is 0.05.

Fig. 3: Same as Fig. 2, but for extreme events selected according to SM. Contour interval is 0.1.

Fig. 4: Same as Fig. 1, but for P seasonal cycle defined as the climatological difference $(P_{max}-P_{min})/2$.

Fig. 5: Composite of surface temperature anomaly difference between cold and warm ENSO events averaged over four seasons for a) CanESM2, b) CCSM4, c) CSIRO-Mk3.6.0, d) IPSL-CM5A-LR, e) MPI-ESM-LR, f) Analysis, g) BCC-CSM1.1, h) CNRM-CM5, i) GFDL-ESM2G, j) HadGEM2-ES, k) MRI-CGCM3, l) NorESM1-M, m) MIROC-ESM, n) MIROC4h, and o) GISS-E2-H in the Tropical Pacific for the historical experiments. Contour interval is 1^{o} C.

Fig. 6: Same as Fig. 5, but for SPI6. Contour interval is 0.3.

Fig.7: Characteristic time of soil moisture for a) CanESM2, b) CCSM4, c) CSIRO-Mk3.6.0, d) IPSL-CM5A-LR, e) MPI-ESM-LR, f) Analysis, g) BCC-CSM1.1, h) CNRM-CM5, i) GFDL-ESM2G, j) HadGEM2-ES, k) MRI-CGCM3, l) NorESM1-M, m) MIROC-ESM, n) MIROC4h, and o) GISS-E2-H for the historical experiments. Contour interval is given by the color bar. The unit is months.

Fig. 8: Difference in SPI6 FOC for positive RCP 8.5 events based on RCP 8.5 climatology minus positive Historical events based on Historical climatology for (a) CanESM2, (b) CCSM4, (c) CSIRO-Mk3.6.0, (d) IPSL-CM5A-LR, and (e) MPI-ESM-LR. (f)-(j) same as (a)-(e) except for negative events. Contour interval is given by the color bar.

Fig. 9: Difference in SPI6 FOC for positive RCP 8.5 events based on Historical climatology minus positive Historical events based on Historical climatology for (a) CanESM2, (b) CCSM4, (c) CSIRO-Mk3.6.0, (d) IPSL-CM5A-LR, and (e) MPI-ESM-LR. (f)-(j) same as (a)-(e) except for RCP 4.5 experiment. Contour interval is given by the color bar.

Fig. 10: Same as Fig. 9, but for negative events.

Fig. 11: Difference in SM FOC for positive RCP 8.5 events based on Historical climatology minus positive Historical events based on Historical climatology for (a) CanESM2, (b) CSIRO-Mk3.6.0, (c) IPSL-CM5A-LR, and (d) MPI-ESM-LR. (e)-(h) same as (a)-(d) except for negative events. Contour interval is given by the color bar.

Fig. 12: Difference in annual mean P climatology for RCP 8.5 minus Historical experiments for a) CanESM2, b) CCSM4, c) CSIRO-Mk3.6.0, d) IPSL-CM5A-LR, e) MPI-ESM-LR, f)

562 BCC- SM1.1, g) CNRM-CM5, h) GFDL-ESM2G, i) HadGEM2-ES, j) MRI-CGCM3, k)
563 NorESM1-M, and l) MIROC-ESM. Contour interval is 0.1 mm day^{-1}. Contours for 0.05
564 mm day^{-1} are added.

565 Fig. 13: Difference in annual mean P for RCP 8.5 minus Historical experiments during JFM for
566 (a) CanESM2, (b) CCSM4, (c) CSIRO-Mk3.6.0, (d) IPSL-CM5A-LR, and (e) MPI-ESM-
567 LR. (f)-(j) same as (a)-(e) but for SSTs.

568

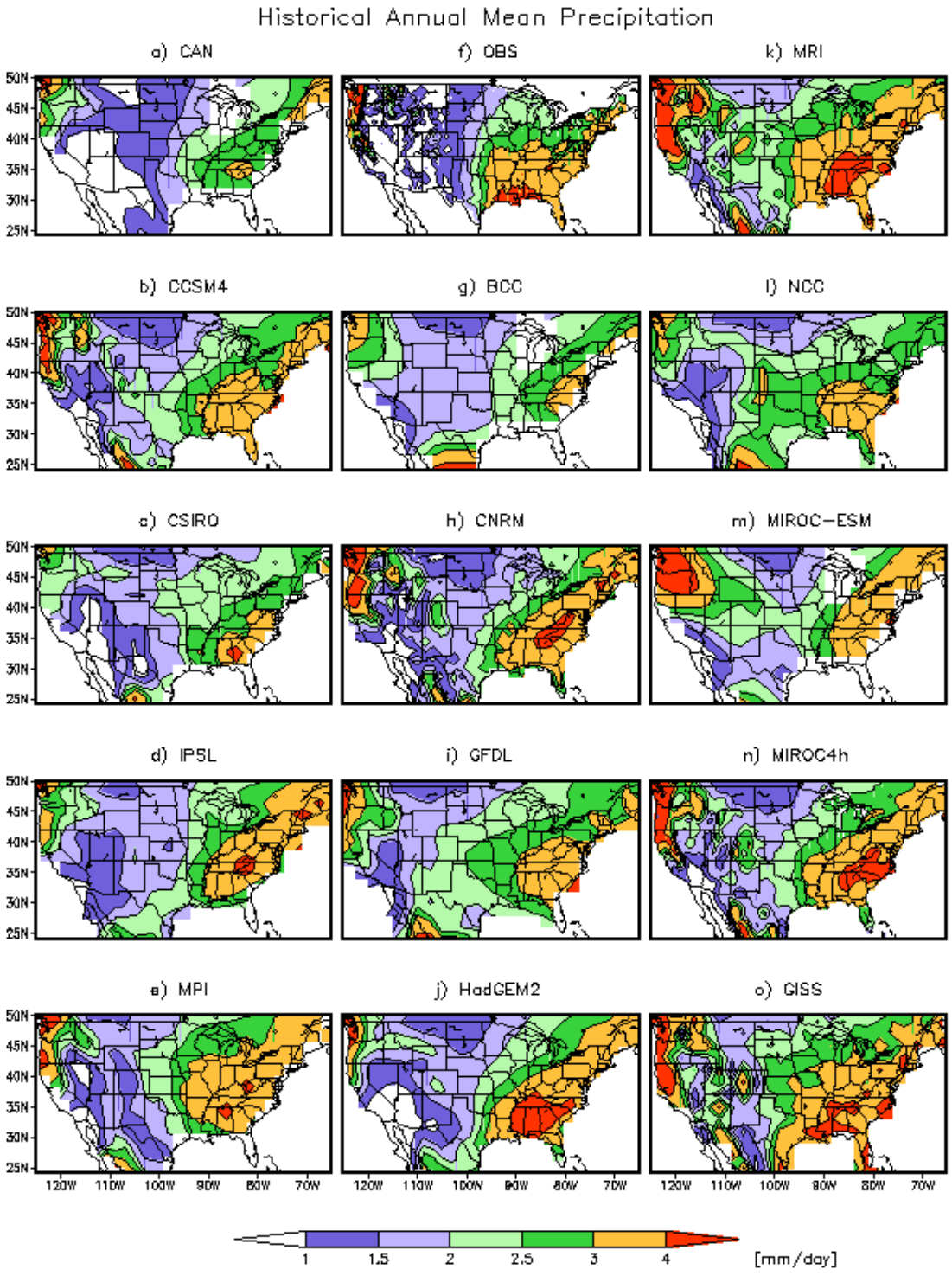

Fig. 1: Annual mean P for a) CanESM2, b) CCSM4, c) CSIRO-Mk3.6.0, d) IPSL-CM5A-LR, e) MPI-ESM-LR, f) Observations, g) BCC-CSM1.1, h) CNRM-CM5, i) GFDL-ESM2G, j) HadGEM2-ES, k) MRI-CGCM3, l) NorESM1-M, m) MIROC-ESM, n) MIROC4h, and o) GISS-E2-H climatology for the historical experiments. Contour interval is given by the color bar.

575 Fig.2

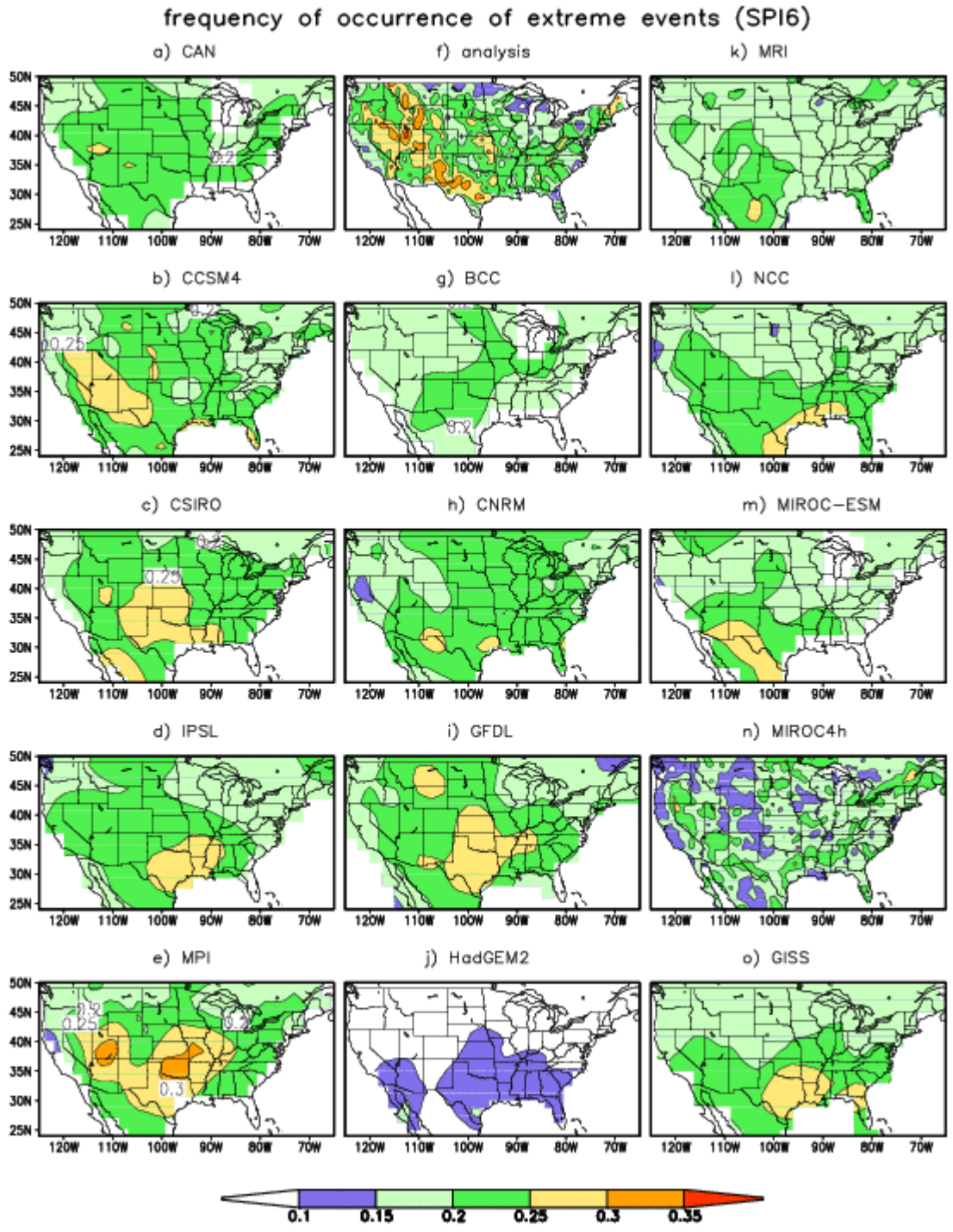

576

577 Fig. 2: Frequency of occurrence (FOC) of extreme events that persist more than 9 months based on SPI6 index
578 averaged over positive and negative events for a) CanESM2, b) CCSM4, c) CSIRO-Mk3.6.0, d) IPSL-
579 CM5A-LR, e) MPI-ESM-LR, f) Observations, g) BCC-CSM1.1, h) CNRM-CM5, i) GFDL-ESM2G, j)
580 HadGEM2-ES, k) MRI-CGCM3, l) NorESM1-M, m) MIROC-ESM, n) MIROC4h, and o) GISS-E2-H for
581 the historical experiments. Contour interval is 0.05.

582 Fig.3

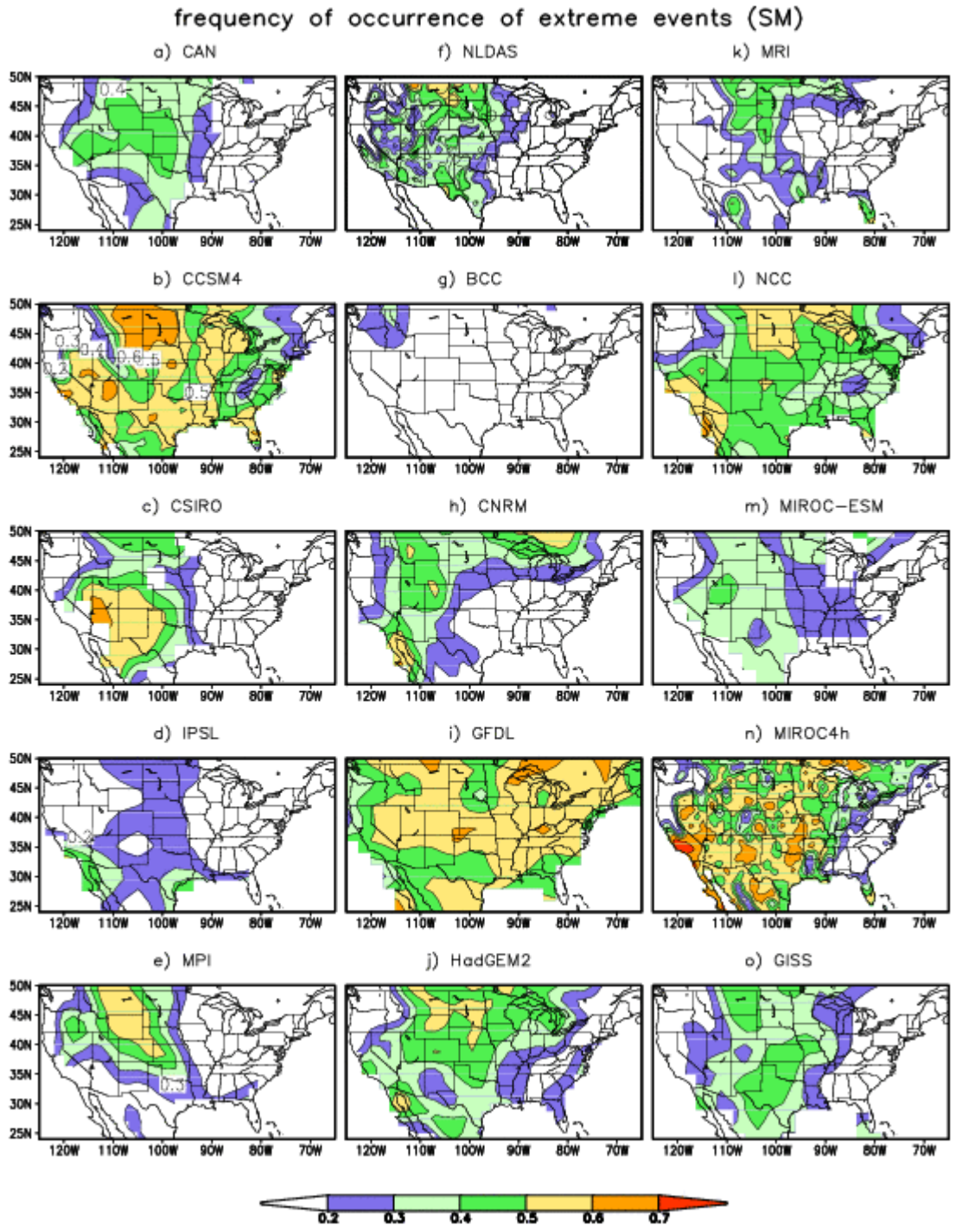

583

584 Fig. 3: Same as Fig. 2, but for extreme events selected according to SM. Contour interval is 0.1.

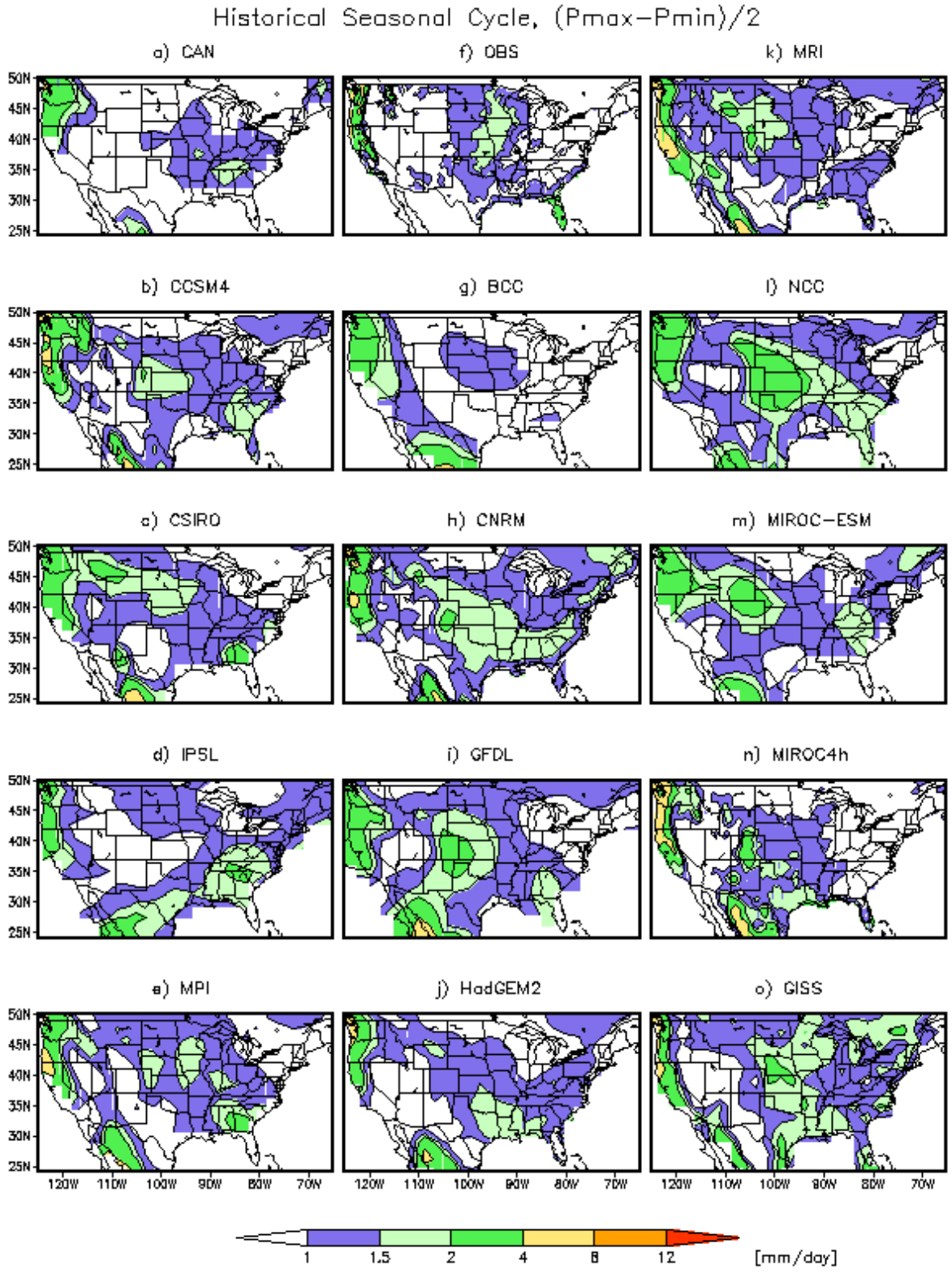

585

586 Fig. 4: Same as Fig. 1, but for P seasonal cycle defined as the climatological difference (P_{max}-
587 P_{min})/2.

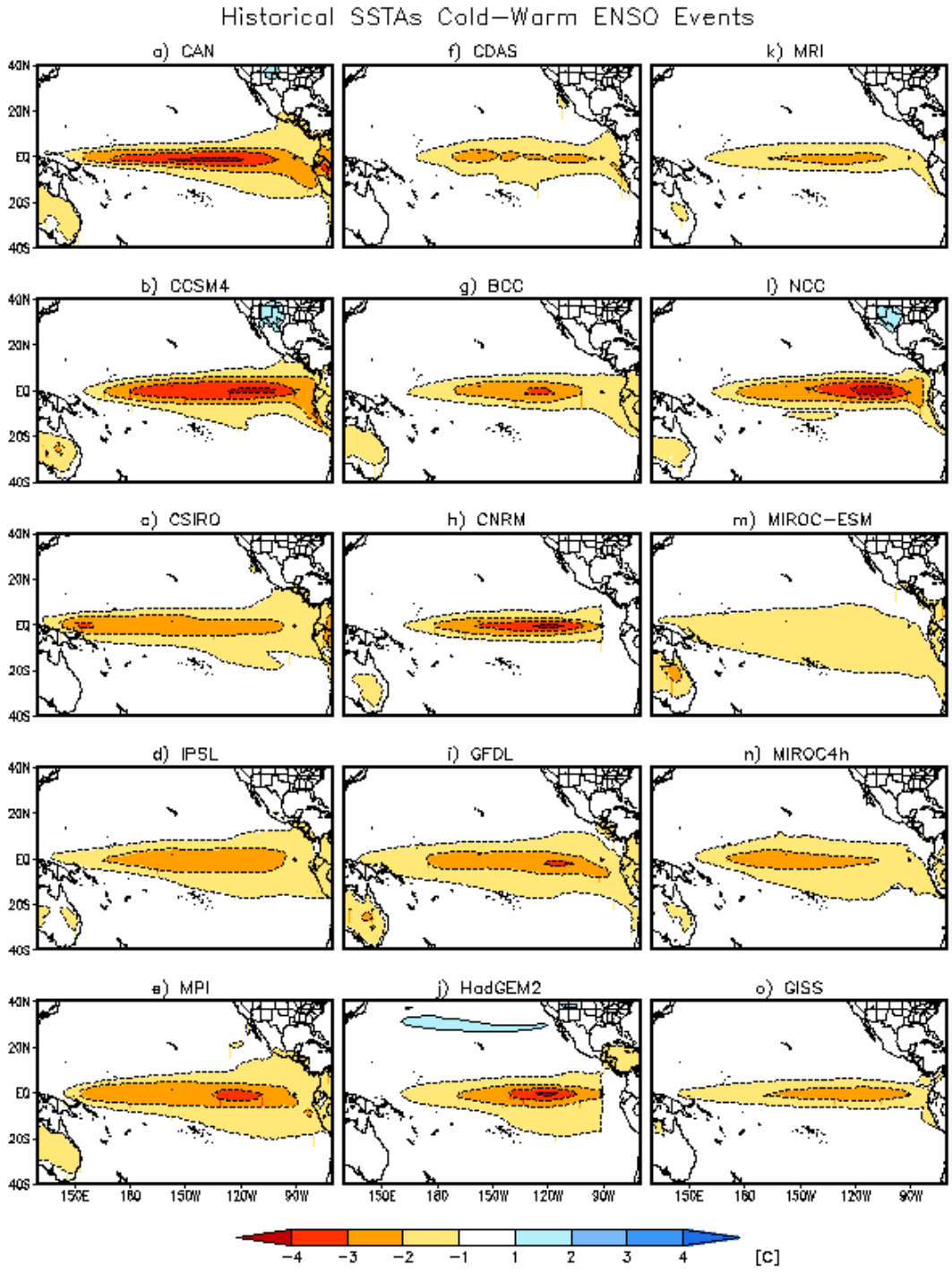

Fig. 5: Composite of surface temperature anomaly difference between cold and warm ENSO events averaged over four seasons for a) CanESM2, b) CCSM4, c) CSIRO-Mk3.6.0, d) IPSL-CM5A-LR, e) MPI-ESM-LR, f) Analysis, g) BCC-CSM1.1, h) CNRM-CM5, i) GFDL-ESM2G, j) HadGEM2-ES, k) MRI-CGCM3, l) NorESM1-M, m) MIROC-ESM, n) MIROC4h, and o) GISS-E2-H in the Tropical Pacific for the historical experiments. Contour interval is 1^{o} C.

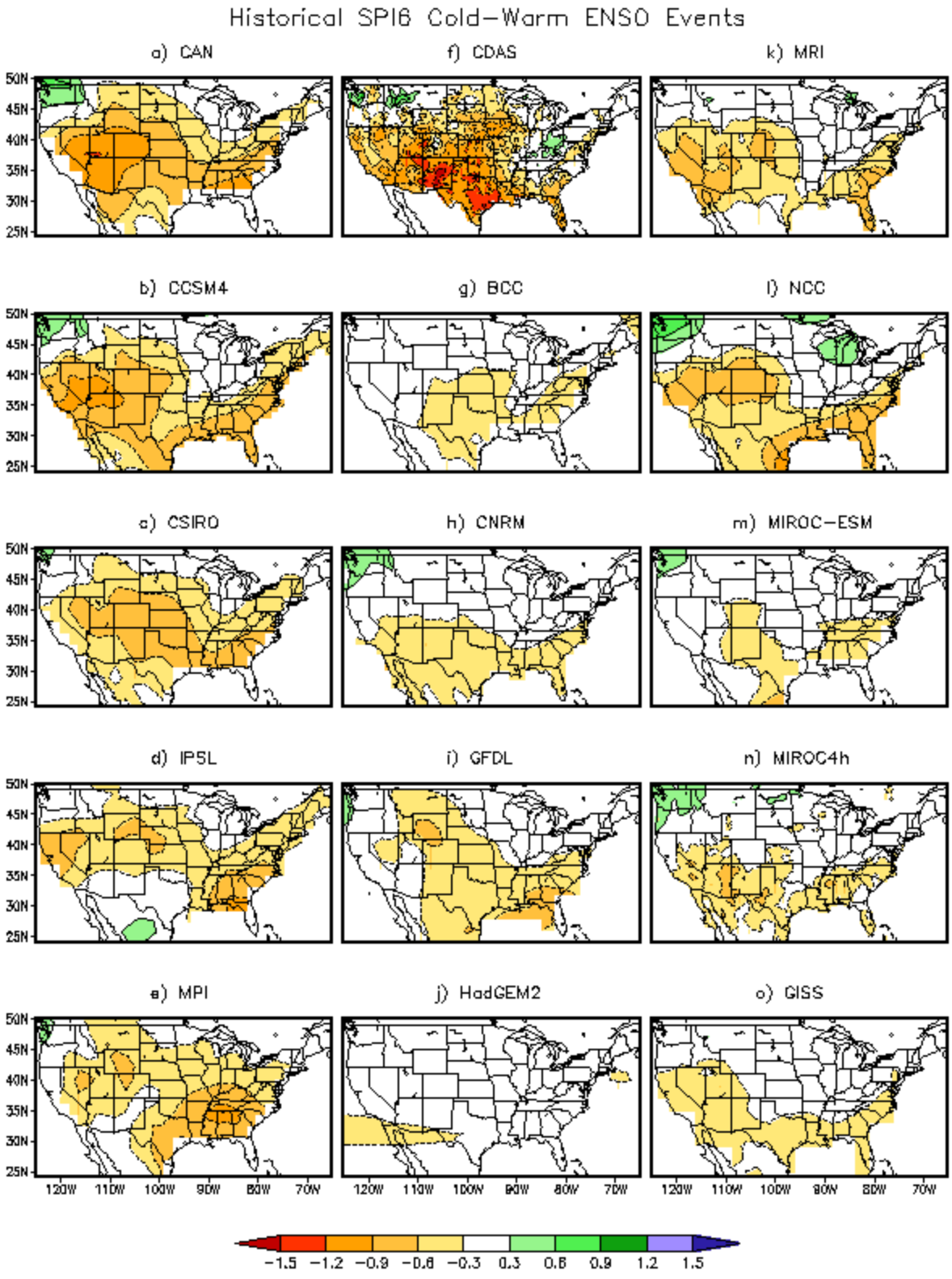

595

596 Fig. 6: Same as Fig. 5, but for SPI6. Contour interval is 0.3.

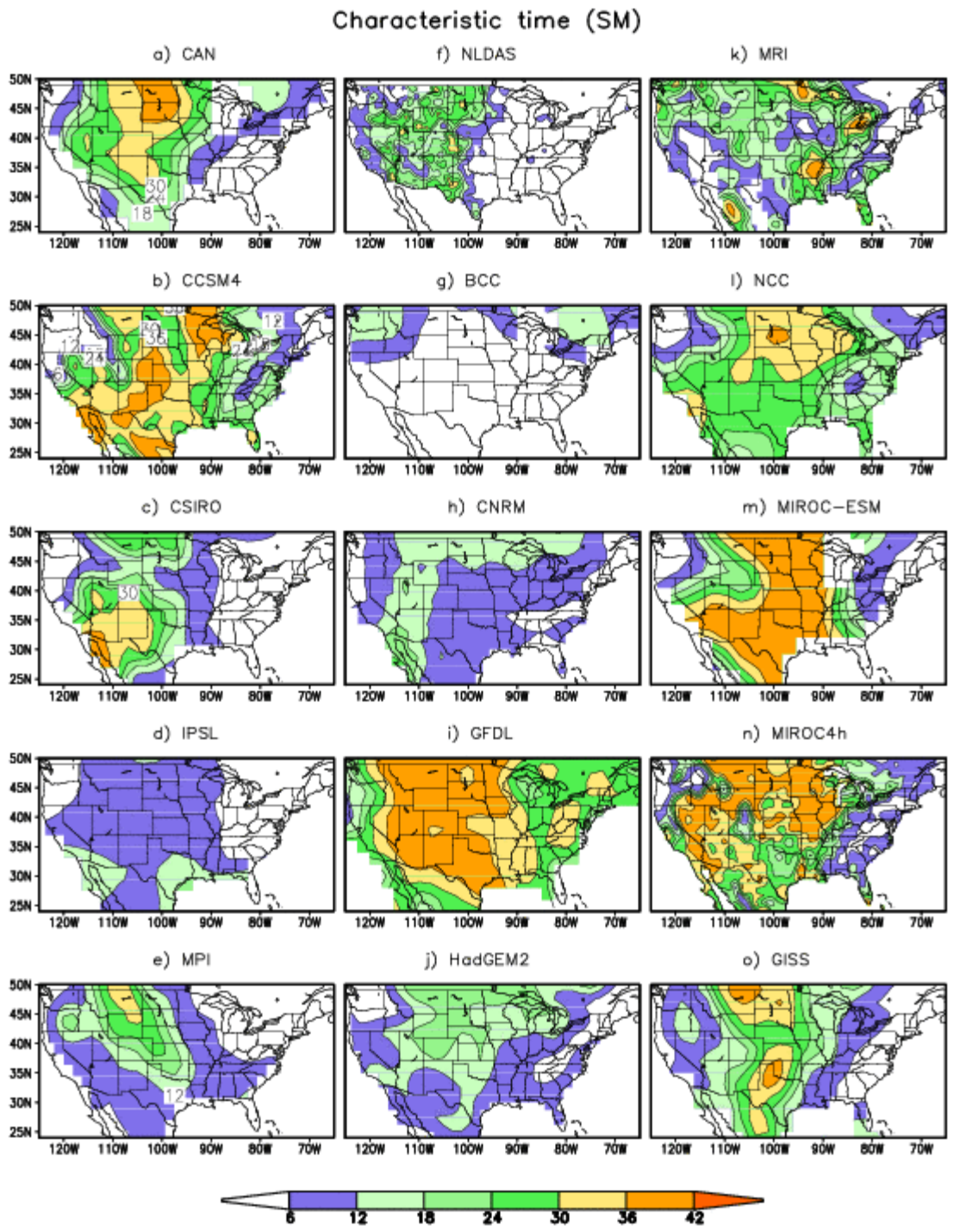

Fig.7: Characteristic time of soil moisture for a) CanESM2, b) CCSM4, c) CSIRO-Mk3.6.0, d) IPSL-CM5A-LR, e) MPI-ESM-LR, f) Analysis, g) BCC-CSM1.1, h) CNRM-CM5, i) GFDL-ESM2G, j) HadGEM2-ES, k) MRI-CGCM3, l) NorESM1-M, m) MIROC-ESM, n) MIROC4h, and o) GISS-E2-H for the historical experiments. Contour interval is given by the color bar. The unit is months.

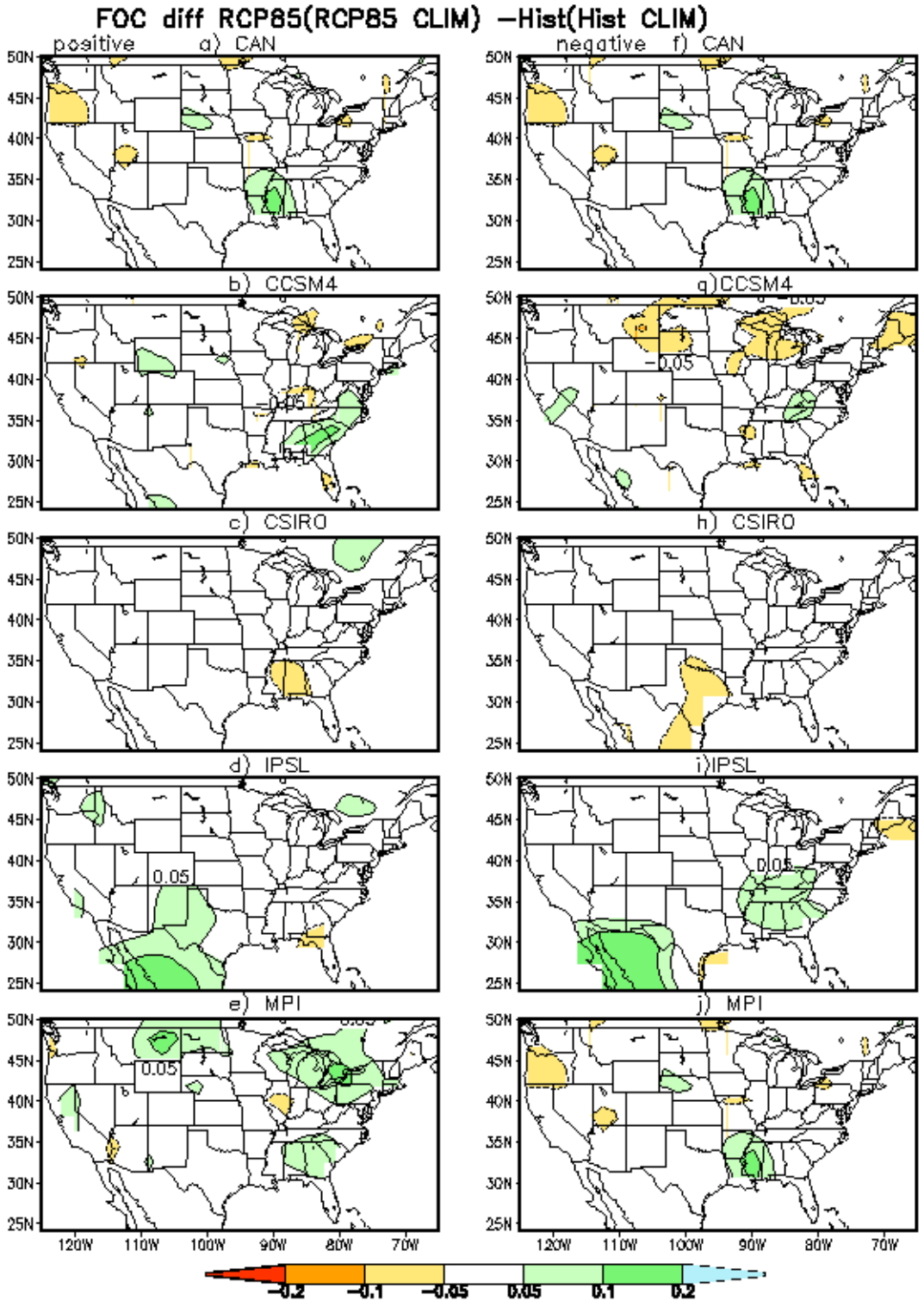

Fig. 8: Difference in SPI6 FOC for positive RCP 8.5 events based on RCP 8.5 climatology minus positive Historical events based on Historical climatology for (a) CanESM2, (b) CCSM4, (c) CSIRO-Mk3.6.0, (d) IPSL-CM5A-LR, and (e) MPI-ESM-LR. (f)-(j) same as (a)-(e) except for negative events. Contour interval is given by the color bar.

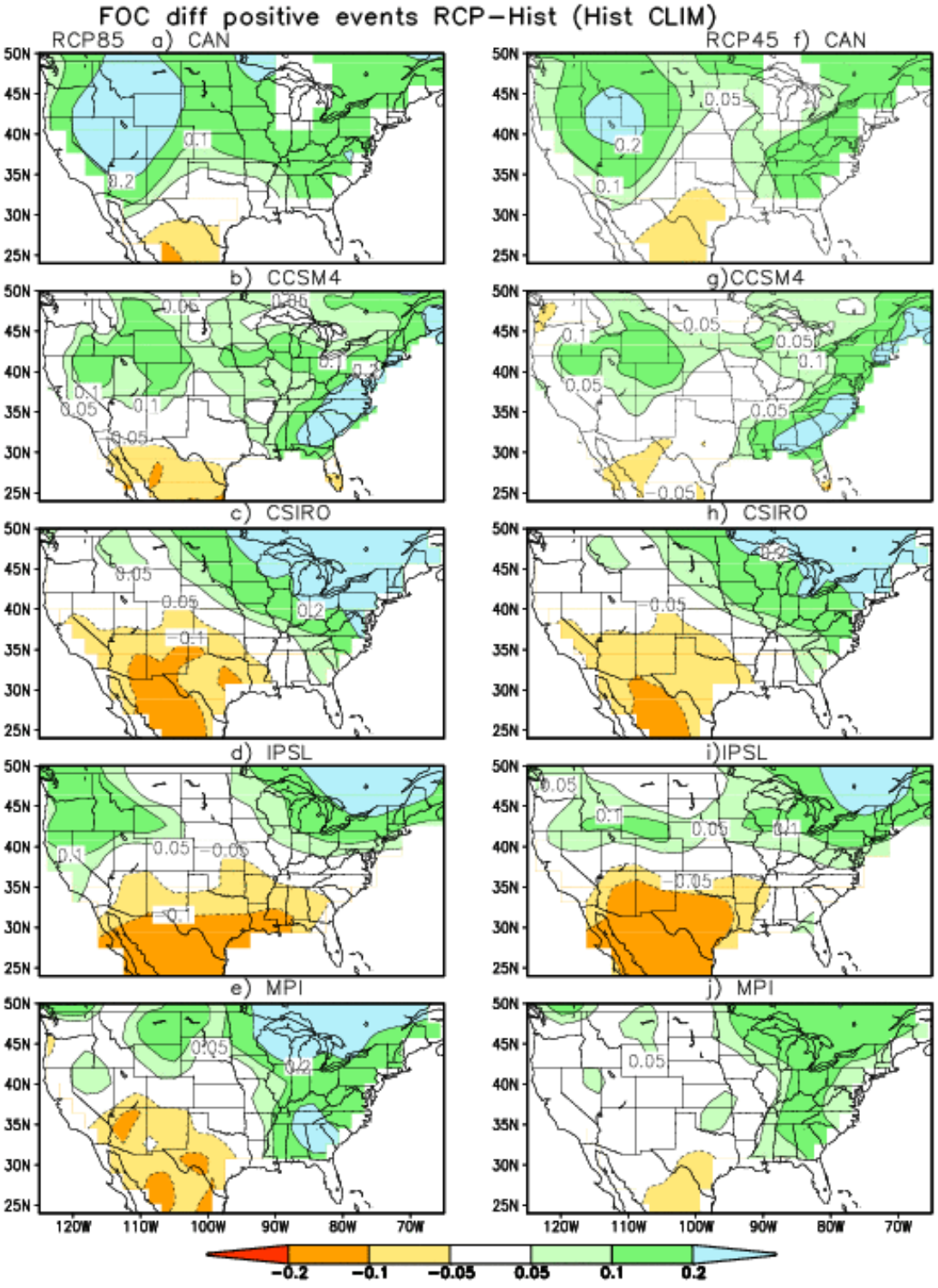

Fig. 9: Difference in SPI6 FOC for positive RCP 8.5 events based on Historical climatology minus positive Historical events based on Historical climatology for (a) CanESM2, (b) CCSM4, (c) CSIRO-Mk3.6.0, (d) IPSL-CM5A-LR, and (e) MPI-ESM-LR. (f)-(j) same as (a)-(e) except for RCP 4.5 experiment. Contour interval is given by the color bar.

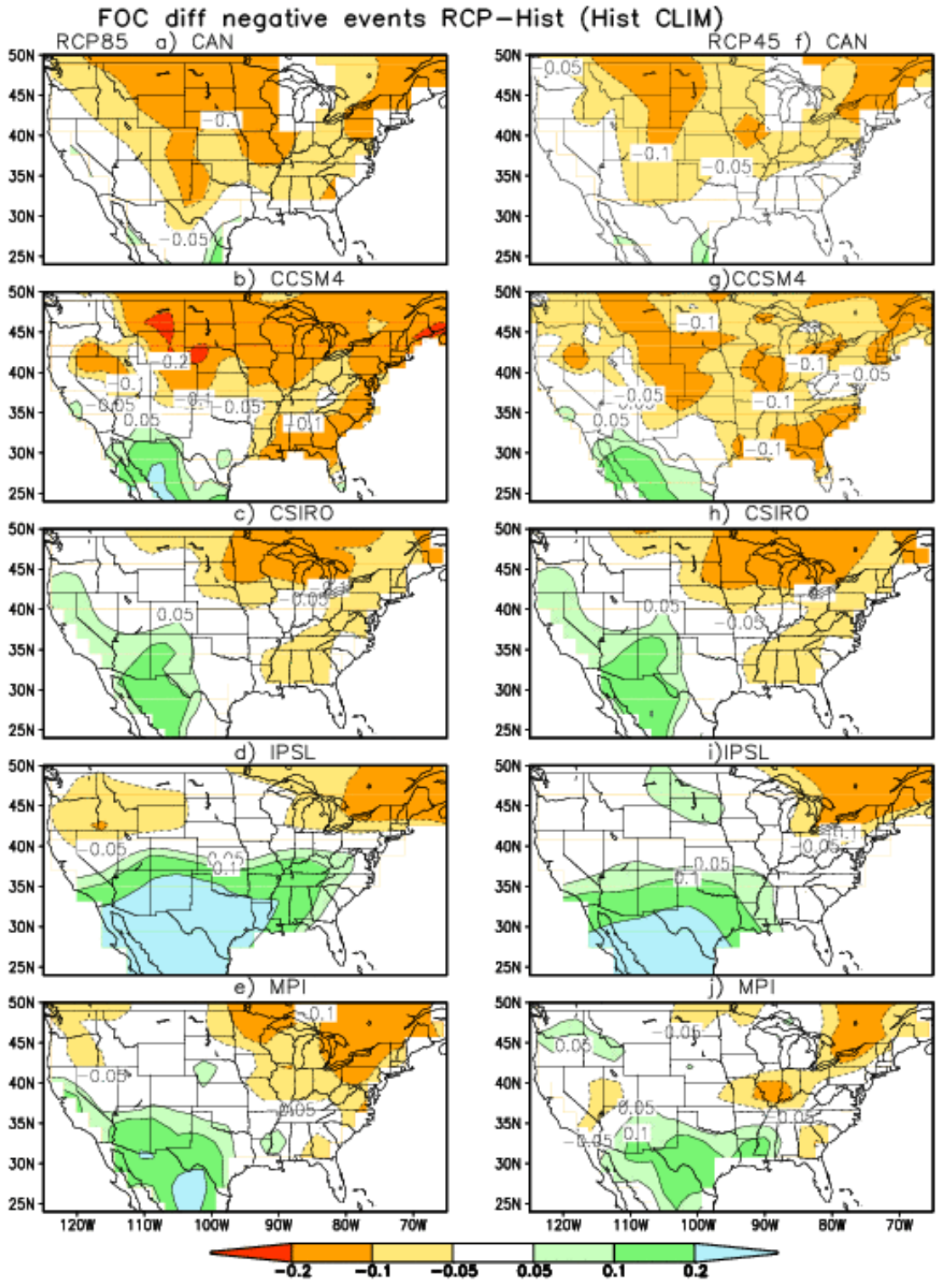

614

615 Fig. 10: Same as Fig. 9, but for negative events.

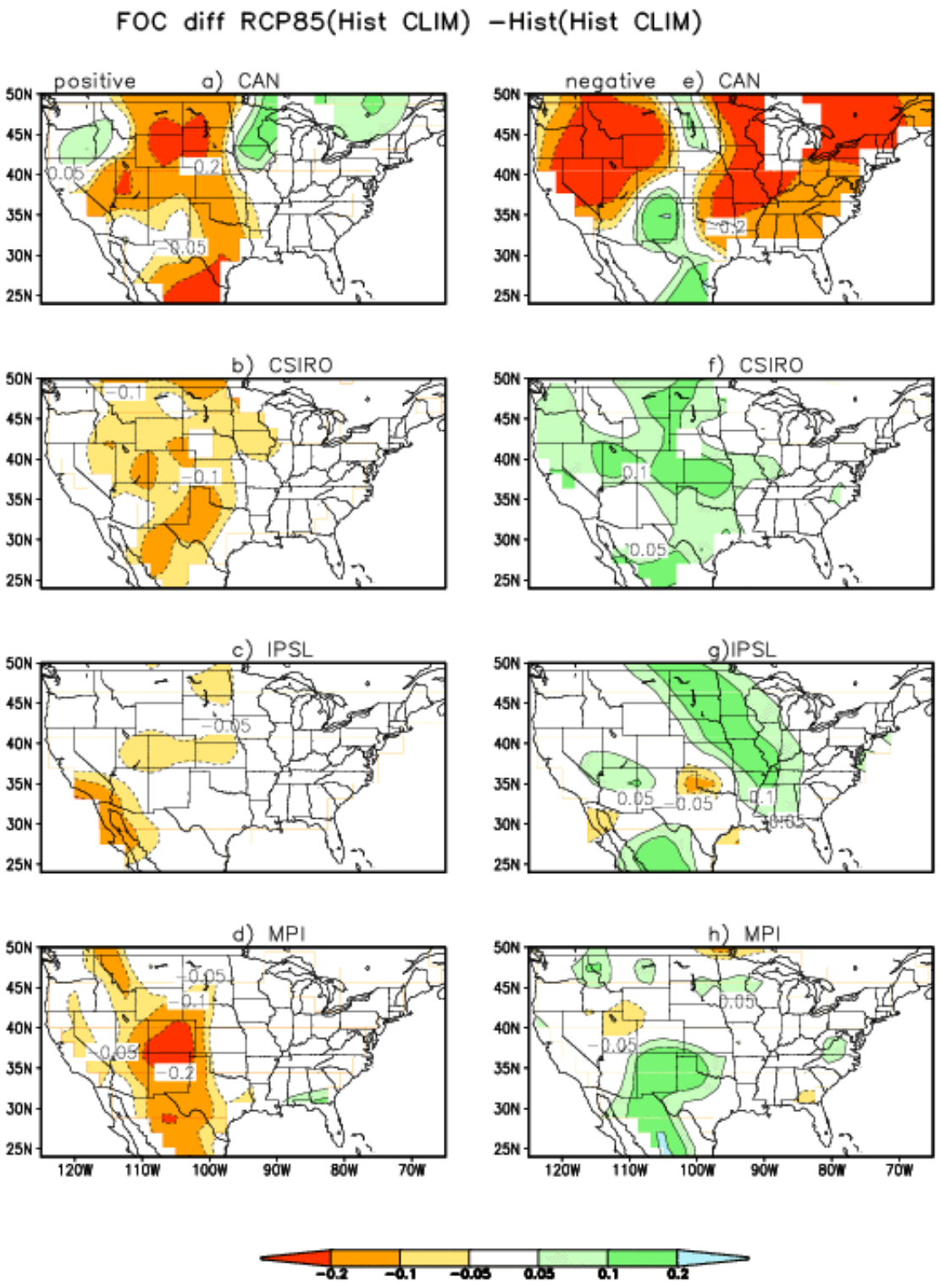

Fig. 11: Difference in SM FOC for positive RCP 8.5 events based on Historical climatology minus positive Historical events based on Historical climatology for (a) CanESM2, (b) CSIRO-Mk3.6.0, (c) IPSL-CM5A-LR, and (d) MPI-ESM-LR. (e)-(h) same as (a)-(d) except for negative events. Contour interval is given by the color bar.

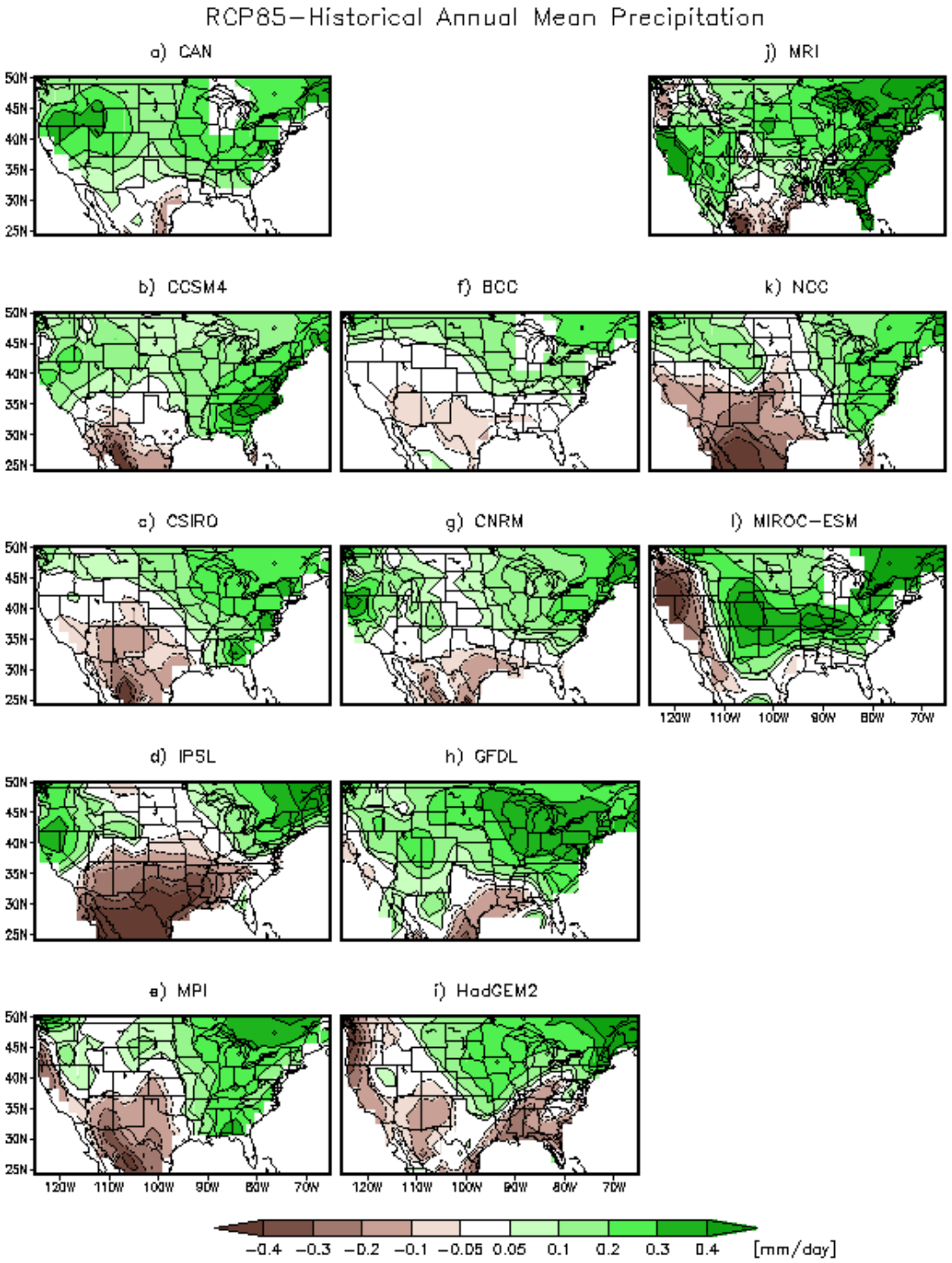

Fig. 12: Difference in annual mean P climatology for RCP 8.5 minus Historical experiments for a) CanESM2, b) CCSM4, c) CSIRO-Mk3.6.0, d) IPSL-CM5A-LR, e) MPI-ESM-LR, f) BCC- SM1.1, g) CNRM-CM5, h) GFDL-ESM2G, i) HadGEM2-ES, j) MRI-CGCM3, k) NorESM1-M, and l) MIROC-ESM. Contour interval is 0.1 mm day^{-1}. Contours for 0.05 mm day^{-1} are added.

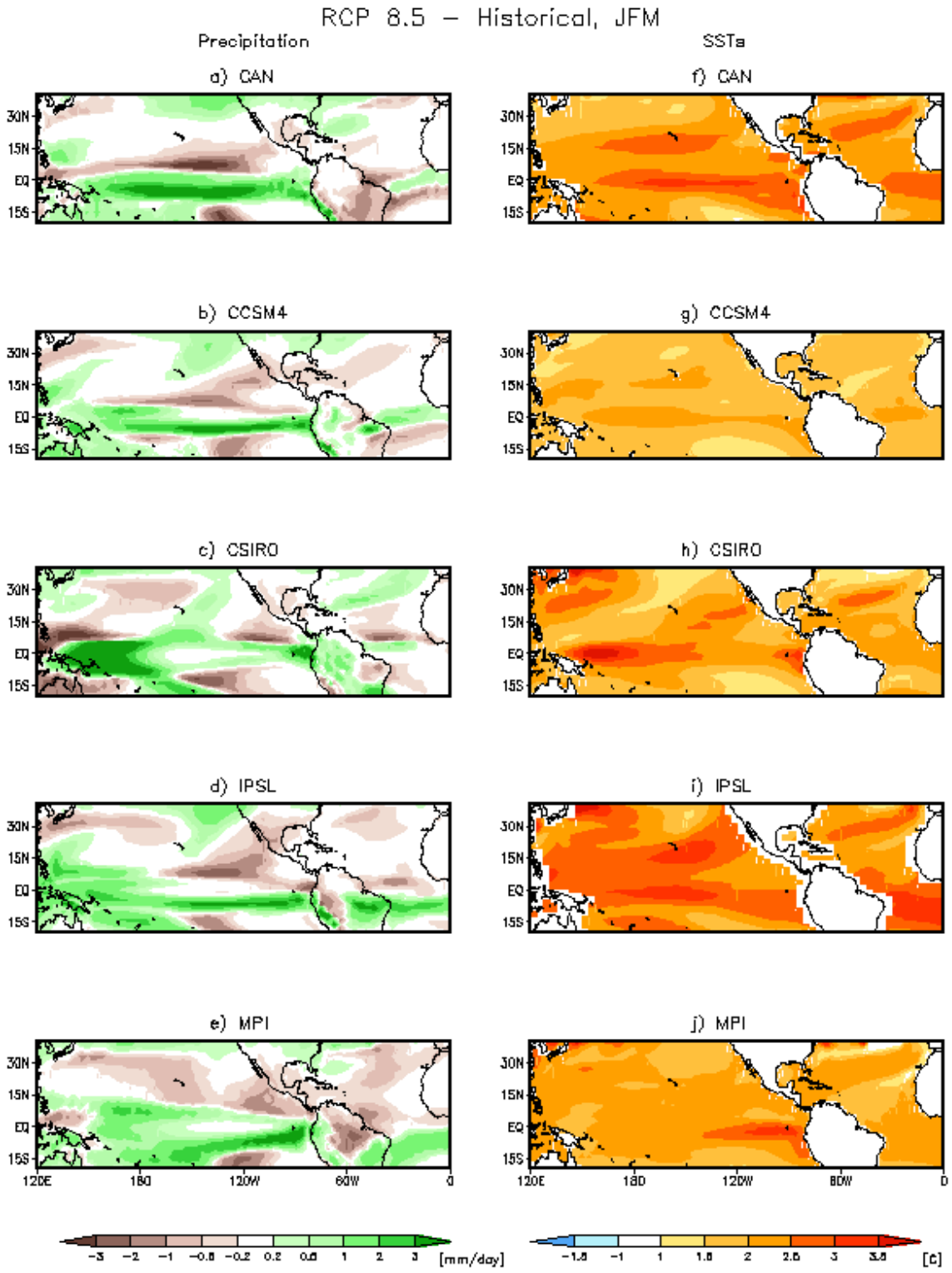

627

628 Fig. 13: Difference in annual mean P for RCP 8.5 minus Historical experiments during JFM for
629 (a) CanESM2, (b) CCSM4, (c) CSIRO-Mk3.6.0, (d) IPSL-CM5A-LR, and (e) MPI-ESM-
630 LR. (f)-(j) same as (a)-(e) but for SSTs.